Supplementary Information

Membrane bending and sphingomyelinase associated sulfatide dependent hypoxic adhesion of sickle mature erythrocytes

Utku Goreke,[1] Erdem Kucukal,[1] Fang Wang,[1] Ran An,[1] Nicole Arnold,[2,3] Erina Quinn,[1,2] Charlotte Yuan, [1,2] Allison Bode, [1,2] Ailis Hill, [1,2] Yuncheng Man,[1] Bryan C. Hambley,[2,3] Robert Schilz[4], Mahazarin Ginwalla,[5] Jane A. Little,[6] Umut A. Gurkan,[1,7,8*]

[1]Department of Mechanical and Aerospace Engineering, Case Western Reserve University, Cleveland, OH, USA

[2]Department of Hematology and Oncology, School of Medicine, Case Western Reserve University, Cleveland, OH, USA

[3]Seidman Cancer Center at University Hospitals Cleveland Medical Center, Cleveland, OH, USA

[4]Division of Pulmonary Medicine, Department of Medicine, University Hospitals Cleveland Medical Center and Case Western Reserve University, Cleveland, OH, USA

[5]Division of Cardiovascular Medicine, Department of Medicine, University Hospitals Cleveland Medical Center and Case Western Reserve University, Cleveland, OH, USA

[6]Division of Hematology/Oncology, Department of Medicine, University of North Carolina, Chapel Hill, NC, USA

[7]Department of Biomedical Engineering, Case Western Reserve University, Cleveland, OH, USA

[8]Case Comprehensive Cancer Center, School of Medicine, Case Western Reserve University, Cleveland, OH, USA

<u>*Corresponding Author:</u>

Umut A. Gurkan, PhD

Case Western Reserve University

Office: Glennan 616B, 10900 Euclid Ave., Cleveland, OH 44106.

Telephone: +1 (216) 368-6447

E-mail: umut@case.edu

1. Supplementary Notes on Semi-Automated Erythrocyte Categorization

Adherent erythrocytes were manually pinpointed in Adobe Photoshop CC® using the count tool. A JavaScript algorithm was used in Adobe Photoshop CC® for saving the pixel locations of the adherent erythrocytes in the microscopy image for further processing. Images of individual erythrocytes were cropped in MATLAB® from fluorescent and phase contrast images of the microchannel using the pixel locations generated by the JavaScript® algorithm. Then orange saturation value of each pixel in each fluorescent channel image was added up to compute the overall orange brightness value. Finally, the algorithm copied each erythrocyte image into a subfolder while appending the brightness value of each image as a prefix to file name. One can navigate to a generated subfolder to analyze the images of individual erythrocytes sorted by their fluorescent intensity.

2. Supplementary Notes on Morphology Analysis of Erythrocytes

Top-hat filtering was applied to remove high and low-frequency noise which diminished the effect of the phase contrast halo around the erythrocytes. The image was then made binary, generating an image that identified only the cell positive pixels. A major axis and an orthogonal minor axis were obtained for each cell by fitting an ellipse to the outer boundary of the cells. Elongation index (EI) was calculated as relative difference,

$$Elongation\ Index\ (EI) = \frac{A - B}{A + B} \tag{1}$$

Equation for EI was set such that EI would be close to one for a line and zero for a circle. EI distribution curves for both reticulocyte and erythrocyte subpopulations were generated for all subjects.

3. Supplementary Notes on Estimation of Accumulated Bending Energy

We estimated the bending energy accumulated on the erythrocyte membrane from two-dimensional images of the sickle erythrocytes. The circumference of the binary images of the erythrocytes was assumed neutral with regards to bending when the erythrocyte shape is fully circular. When the erythrocyte is elongated the shape is approximated by two overlapping circles. Radii of these two curves define the rate of change of curve along the periphery of the erythrocyte. Then accumulated bending energy (f_b) required to deform a membrane from its neutral curvature J_n to a mean curvature J_m is given by can be estimated by,[1,2]

$$f_b = \frac{1}{2}\kappa(J_m - J_n)^2 \tag{2}$$

We calculated the bending energies of adhered erythrocytes by obtaining J_n values from normally distributed HbAA erythrocytes. The local bending energy depends on the bending rigidity κ. Assuming constant $\kappa = 9 \times 10^{-19} J$, the local bending energy per unit area is a function of the local curvature R.[3]

4. Supplementary Notes on Outlier Analysis

We performed the Dixon's Q ratio outlier test to determine possible outliers in the hypoxic adhesion data of subjects. Normal distribution assumption is required to classify a data point as lying outside the range of expected values.[4] Since our data was non-normal with 41 patients (N_{IPS}=23 and $N_{no\text{-}IPS}$ =18, Anderson-Darling, p<0.005 both), the data was preprocessed by Box-

Cox transformation in R for normalization approximation. Based on outlier analysis one outlier data point from each group was identified with mild significance (IPS group, 18368 total RBC adhesion under hypoxia, Dixon's Q ratio, p=0.084 and no-IPS group, 3504 total RBC adhesion under normoxia, Dixon's Q ratio, p=0.073). When these two points were removed, adhesion data for both groups became normally distributed (Anderson-Darling, p=0.364 for IPS and p=0.093 for no-IPS group). To search additional outliers Box-Cox normalization was not performed on normally distributed data and no outliers were identified (Dixon's Q ratio, p=0.085 for IPS and p=0.066 for no-IPS group). We performed the same procedure for assessing possible outliers in erythrocyte hypoxic adhesion data for 15 patients. Similarly, the adhesion data were non-normal (Anderson-Darling, p<0.001) but there were no outliers after Box-Cox transformation (Dixon's Q ratio, p=0.330). We opted to disseminate the results and clinical phenotype of the subjects without these two data points as well.

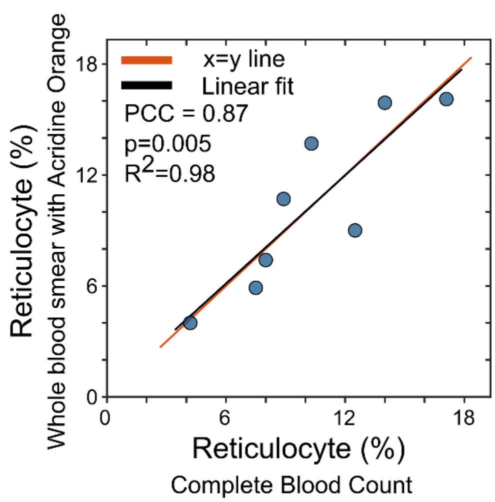

Supplementary Figure S1. Categorization accuracy of adherent sRBCs as reticulocytes and erythrocytes in normoxic and hypoxic microscale flow. Clinical laboratory results for reticulocytes show agreement with the acridine orange staining of whole blood smears. x=y line denotes the perfect agreement fit. *PCC: Pearson Correlation Coefficient, p-value and R-squared are calculated from linear regression*

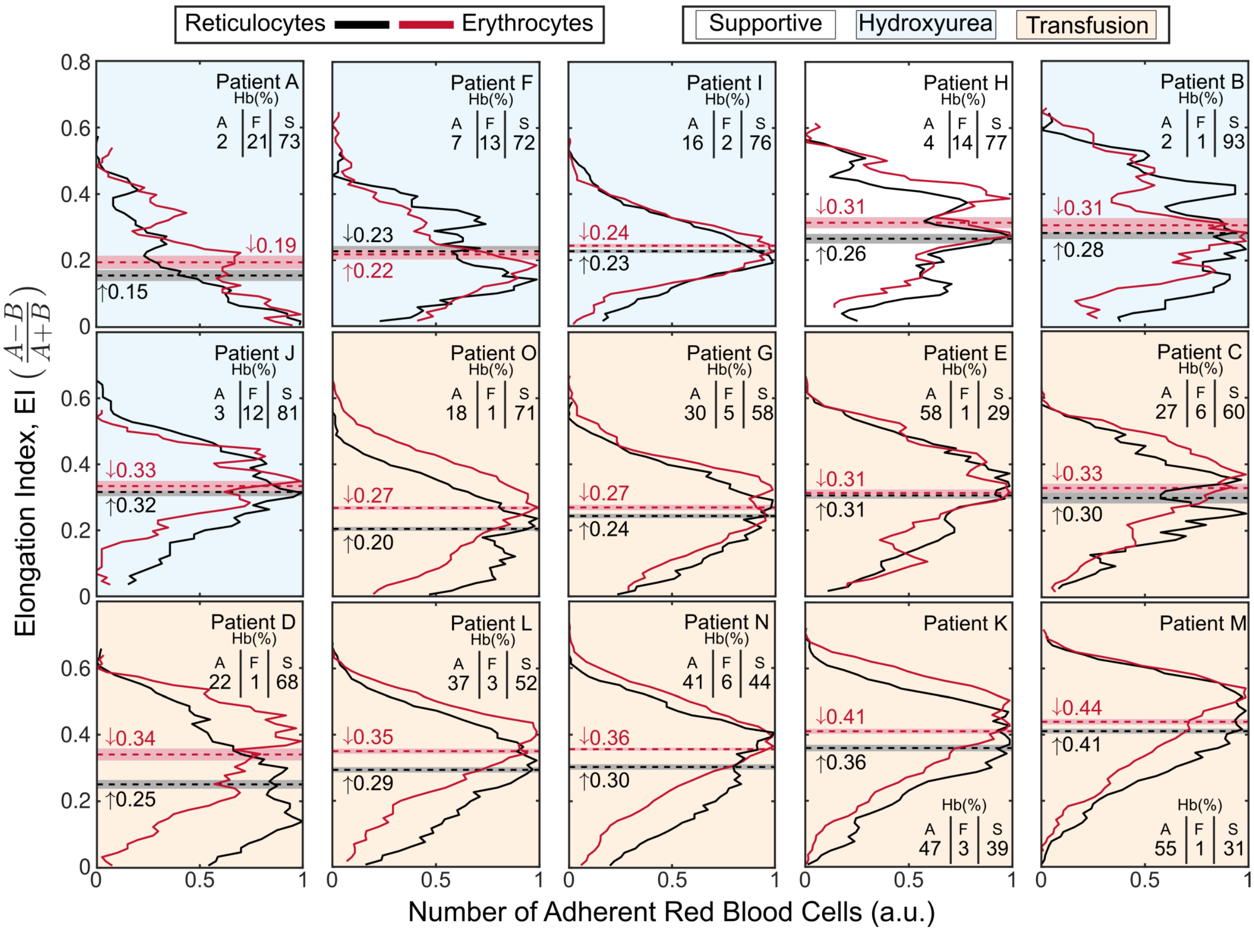

Supplementary Figure S2. Elongation index (EI) profiles of each homozygous SCD subject (N=15) shown individually. Subjects are grouped based on their regular treatment types as non-transfused and transfused and are shown in increasing order of EI internally within each group from left to right and top to bottom. Shown in insets the below patient identification letters hemoglobin percentages of each sample. The horizontal bars denote the mean and the 95% confidence interval of the mean. The mean EI of erythrocytes and reticulocytes are significantly different based on one-way ANOVA when the confidence intervals do not overlap.

Supplementary Table S1. Clinical phenotype of the study population with and without a history of intrapulmonary shunting (IPS) when the highest adhesion data points in each group are romved.

	Subjects with h/o IPS (mean ± SD)	Subjects without known h/o IPS (mean ± SD)	p-value
N (Number of subjects)	22	17	
Age (years)	33.9 ± 10.0	31.6 ± 9.6	0.335*
Gender	**M=14 / F=8**	**M=5 / F=12**	**0.034†**
Total RBC (erythrocyte+reticulocyte) Adhesion in Normoxia	**913 ± 716**	**245 ± 216**	**0.002***
Total RBC (erythrocyte+reticulocyte) Adhesion in Hypoxia	**2638 ± 1934**	**960 ± 846**	**0.006***
Hgb (g/dL)	8.4 ± 1.8	8.2 ± 0.9	0.496*
WBC (10^9/L)	11.3± 2.8	10.0 ± 3.9	0.233**
Absolute Neutrophil Count (10^6/L)	6747± 2624	5910 ± 2899	0.311**
Platelet Count (10^9/L)	353.1 ± 124.8	317.0 ± 112.2	0.213**
Mean Corpuscular Volume (MCV)	92.0 ± 10.1	94.0 ± 12.0	0.670*
Reticulocyte Count (10^9/L)	**452.4 ± 186.8**	**282.3 ± 202.4**	**0.009****
LDH (U/L)	**477.7 ± 295.6**	**300.4 ± 151.5**	**0.009***
Ferritin (μg/L)	2376 ± 3048	2440 ± 2635	0.530*
Hb S (%)	62.6 ± 22.6	55.4 ± 22.3	0.271*
Hb A (%)	25.0 ± 21.8	30.2 ± 25.2	0.509*
Hb F (%)	4.6 ± 4.7	7.0 ± 6.5	0.191*
Recently transfused (HbA>10%)	13/22	11/17	0.721†
h/o ‘in vivo’ Hb desaturation (nocturnal or exertional)	**17/22**	**7/17**	**0.011†**

h/o is abbreviation for history of
* Calculated based on non-parametric Mann-Whitney Test
** Calculated based on one-way ANOVA
† Calculated based on Chi-square

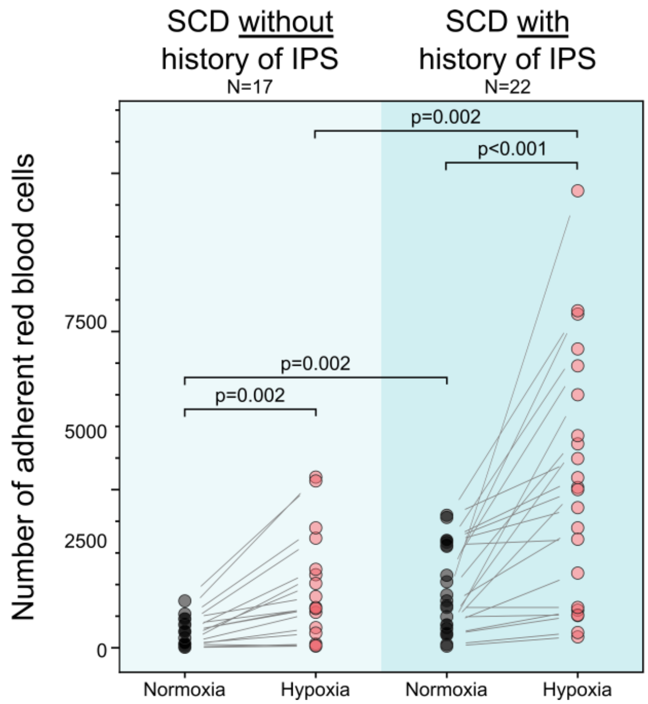

Supplementary Figure S3. Representation of the data without the highest adhesion data points in each group. Hypoxia enhanced total RBC adhesion is associated with intrapulmonary shunting (IPS) in subjects with HbSS SCD. RBCs from both subject groups display a significant increase in adhesion under hypoxia compared to normoxia, and normoxic and hypoxic adhesion of RBCs are significantly different between IPS and no-IPS groups. *$N_{no\text{-}IPS}$=17, N_{IPS}=21, p-values were calculated using Mann-Whitney Test and one-way ANOVA for non-normal and normal data, respectively.*

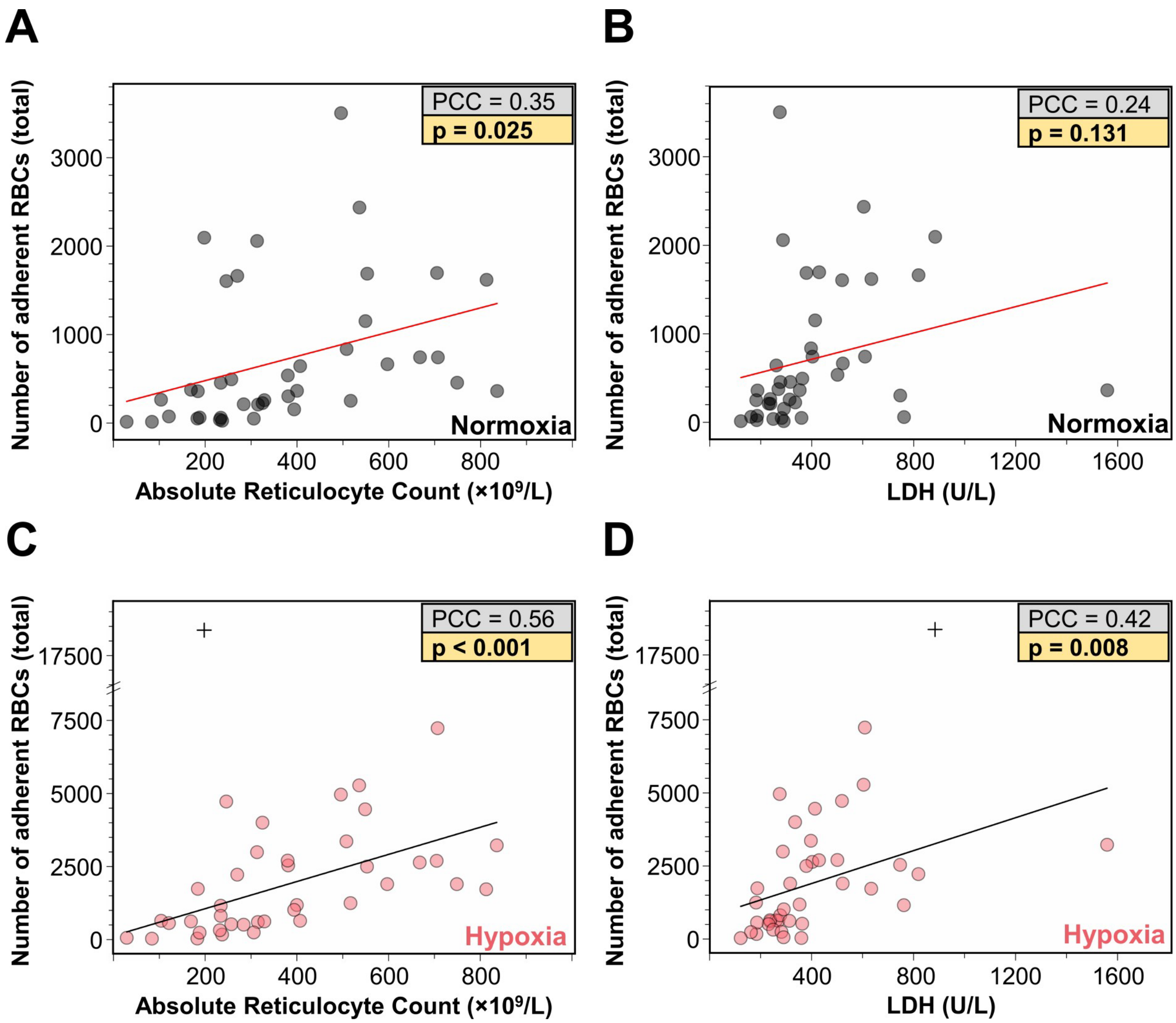

Supplementary Figure S4. We observed significantly increased total RBC (RBC, reticulocytes + erythrocytes) adhesion to laminin (LN) under both normoxia and hypoxia in subjects with more severe disease phenotype marked by higher lactate dehydrogenase (LDH) and absolute reticulocyte count (ARC). Correlations of total RBC adhesion to LN with ARC and LDH under normoxia **(A-B)** and under hypoxia **(C-D)**. *N=41, Data points denoted by cross signs are not included in the analysis. PCC: Pearson Correlation Coefficient, p-values were obtained from linear regression model.*

Transfused HbAA RBCs do not confound SCD whole blood RBC adhesion to laminin

We inspected RBC adhesion to laminin (LN) for transfused HbA RBCs that are present in SCD whole blood samples in varying percentages. RBC units are stored for at most six weeks in the blood bank.[5] We tested normoxic adhesion of HbA RBCs to LN from a single blood unit, sampling over 6 weeks. Normoxic adhesion of HbA-containing stored RBCs increased with time, but remained at a relatively low level compared with normoxic adhesion from sRBCs (**Supplementary Figure 6A**, 232 vs. 728±125). Finally, we investigated the relationship of HbS percentage with RBC adhesion to LN. We found no significant association between HbS percentage and sRBC adhesion to LN under normoxia (**Supplementary Figure 6B**, p=0.514, PCC=-0.11, linear regression and Pearson correlation) nor hypoxia (**Supplementary Figure 6B**, p=0.868, PCC=-0.03, linear regression and Pearson correlation).

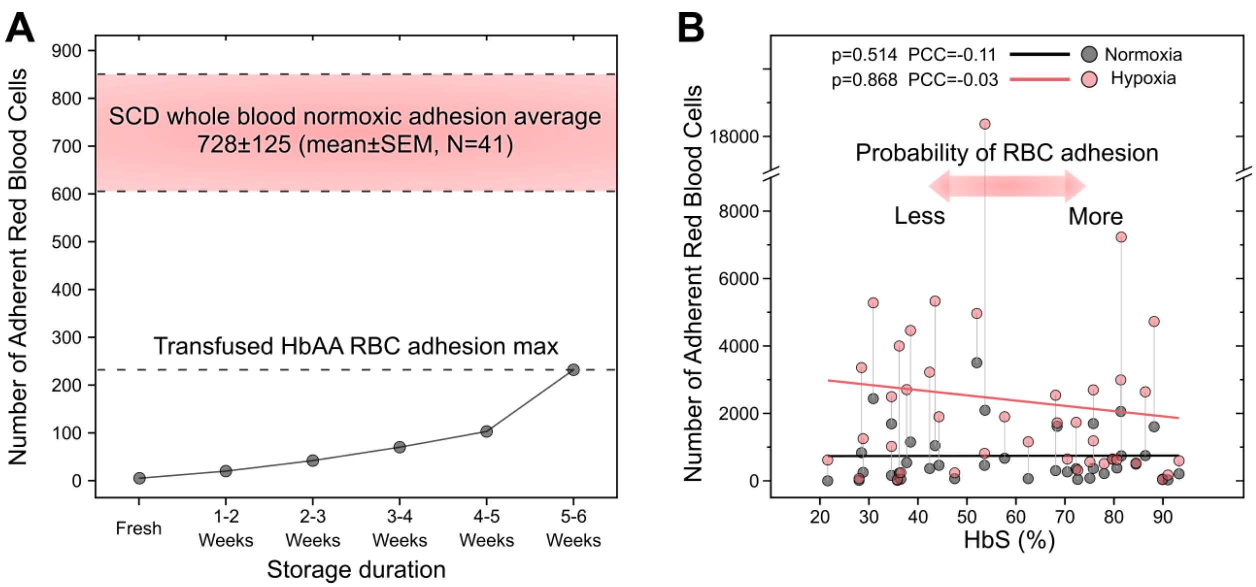

Supplementary Figure S5. Evaluation of red blood cell (RBC) adhesion assay feasibility (A) HbA-containing RBCs that were used for transfusion becomes increasingly more adherent to laminin (LN) over a typical duration of storage in a blood bank. The average of RBC adhesion of SCD whole blood samples are shown for comparison. **(B)** Hypoxic and normoxic adhesion of 41 SCD patients were visualized along with HbS% that is measured from the same sample. Lines connect the hypoxic and normoxic adhesion values of the same SCD patient. The more elevated HbS%, the higher probability of RBC adhesion in RBC adhesion assay due to greater number of sickle RBCs interacting with the protein functionalized surface. However, neither normoxic nor hypoxic RBC adhesion is associated with HbS%, suggesting that RBC adhesion depends on patient specific factors rather than HbS% only. *PCC: Pearson Correlation Coefficient, p-values are calculated from one-way ANOVA and linear regression.*

REFERENCES

1. Helfrich W. Elastic properties of lipid bilayers: theory and possible experiments. *Zeitschrift für Naturforschung c*. 1973;28(11-12):693-703.

2. López DJ, Egido-Gabas M, López-Montero I, et al. Accumulated bending energy elicits neutral sphingomyelinase activity in human red blood cells. *Biophys J*. 2012;102(9):2077-2085.

3. Geekiyanage NM, Balanant MA, Sauret E, et al. A coarse-grained red blood cell membrane model to study stomatocyte-discocyte-echinocyte morphologies. *PLoS One*. 2019;14(4):e0215447.

4. Dean RB, Dixon WJ. Simplified Statistics for Small Numbers of Observations. *Anal Chem*. 1951;23(4):636-638.

5. Rapido F, Brittenham GM, Bandyopadhyay S, et al. Prolonged red cell storage before transfusion increases extravascular hemolysis. *J Clin Invest*. 2017;127(1):375-382.